Simulation of stratified mixing in thin aspect ratio domain using a spect ral element method: Handling small scale noise and improving the iterative Poisson solver

Mohamed Iskandarani
Tamay Özgökmen
Weiwei Zhang
Silvia Matt

Rosenstiel School of Marine and Atmospheric Science, University of Miami

August 18, 2009

Overview

Motivation

The Model
- Model Features

Estimating DG-induced mixing
- Estimating Implicit Mixing

Boutique solver
- Domain Decomposition Algorithm
- Remarks

Conclusion

Gravity Current Simulation

- Mixing and entrainment in gravity currents transform source waters into deep and intermediate waters
- Carried by large scale ocean currents O(10-100 km).
- Dynamical scales of mixing instabilities are small compared to oceanic scales: SGS needed to model mixing.
- Parameterization need to be validated against observation and DNS-type simulation.
- increase modeled *Re* or increase size of computational domain to follow evolution of gravity current.
- Process-oriented studies in idealized channels

Gravity Current Simulation

$$
\begin{aligned}
\frac{\partial \zeta}{\partial t} + \vec{u} \cdot \nabla \zeta &= \frac{1}{R_e} \nabla^2 \zeta - \frac{1}{F_r^2} \rho_x, \quad R_e = \frac{UL}{\nu}, \quad F_r = U \left(g \frac{\Delta \rho}{\rho_0} L \right)^{-\frac{1}{2}} \\
\nabla^2 \psi + \zeta &= 0 \\
\frac{\partial \rho}{\partial t} + \vec{u} \cdot \nabla \rho &= \frac{1}{P_r\, R_e} \nabla^2 \rho, \quad P_r = \frac{\nu}{\nu_\rho}
\end{aligned}
$$

- Currently a 2D model built on Boussinesq NS equations in a $\zeta - \psi$ formulation.
- A salt-like tracer evolves according to an advection diffusion equation, and provides buoyancy forcing.

Model Highlights

- $\zeta - \psi$ equations discretized using spectral elements.
  - Dual paths *h-p* convergence rates for smooth solutions
  - Excellent scalability on parallel computers
  - Phase fidelity and no numerical dissipation.
- Poisson equation solved using substructing and PCG on the Schur complement.
- Tracer equation discretized with spectral element DGM.
  - Discontinuous interpolation & local mass matrices.
  - Well-suited to advection-dominated flows.
  - Upwind flux bias controls Gibbs oscillations

Gravity Current Simulation at $R_e = 50,000$

Impact of varying inlet current height

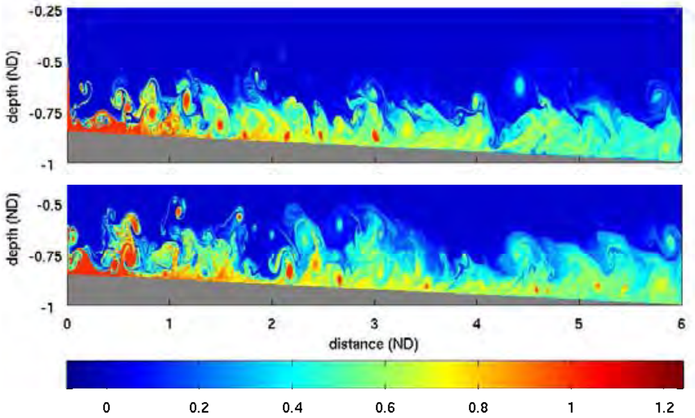

steady

varying

Grid: 300x50 elements of degree 8 with refinement near bottom

Transport in Density Classes $R_e = 50,000$

Impact of varying inlet current height

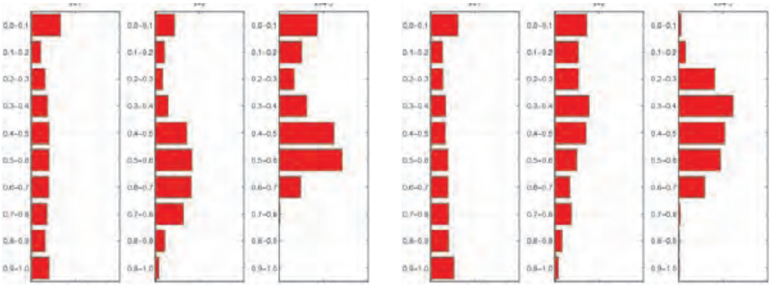

steady varying

- Densest water mixed in both cases
- In steady case most transport is in 0.4-0.6 class
- In time-varying case transport is in 0.2-0.4 class

Questions

- Can DG deliver reliable estimate of mixing?
  Convergence analysis
- Can we increase domain size while keeping cost low and/or high scalability?
  Improve iterative solver

Estimating Implicit Mixing in DG solution

- How much of the mixing is spurious (numerical)
- Sequence of CG/DG solutions to verify convergence
  - $R_e = 2,000$, $P_r = 7$.
  - $R_e = 10,000$, $P_r = 7$.
- Metrics for judging solution
  - monotonicity of ρ:

$$\min[\rho(\vec{x}, t = 0)] \leq \rho(\vec{x}, t) \leq \max[\rho(\vec{x}, t = 0)]$$

  - density classes
  - Energy budget

Energy Equation for Closed insulated Domain

$$\frac{d}{dt}\left(\int_A E\, \mathrm{d}A\right) = -\int_A \left[\frac{\zeta^2}{Re} + \frac{\nabla z \cdot \nabla \rho}{R_e P_r F_r^2}\right] \mathrm{d}A \qquad (1)$$

$$E = E_k + E_p = \frac{\vec{u}\cdot\vec{u}}{2} + \frac{\rho z}{F_r^2} \qquad (2)$$

$$E_p = E_a + E_b = \frac{\rho(z - z_*)}{F_r^2} + \frac{\rho z_*}{F_r^2} \qquad (3)$$

- z_*: vertical position after adiabatic ρ-redistribution
- E_b: Background potential energy
  responds only to diabatic processes
- E_a: Available potential energy
  responds to reversible adiabatic processes only.

R_e	$K_x \times K_y \times N$	DG-Time	CG-time
2,000	020 $\times$ 04 $\times$ 06	30.00	30.00
2,000	025 $\times$ 05 $\times$ 06	16.00	
2,000	030 $\times$ 06 $\times$ 06	16.00	
2,000	040 $\times$ 08 $\times$ 06	80.00	7.32
2,000	040 $\times$ 08 $\times$ 07	80.00	
2,000	040 $\times$ 08 $\times$ 08	80.00	
2,000	040 $\times$ 08 $\times$ 09	80.00	
2,000	040 $\times$ 08 $\times$ 09	80.00	
2,000	080 $\times$ 16 $\times$ 06	82.00	95.00
2,000	080 $\times$ 16 $\times$ 07	80.00	
2,000	080 $\times$ 16 $\times$ 08	80.00	
2,000	080 $\times$ 16 $\times$ 09	80.00	
2,000	160 $\times$ 32 $\times$ 06	80.00	80.00
2,000	160 $\times$ 32 $\times$ 06	104.00	
2,000	160 $\times$ 32 $\times$ 07	80.00	
2,000	160 $\times$ 32 $\times$ 08	80.00	
2,000	160 $\times$ 32 $\times$ 09	80.50	
2,000	320 $\times$ 64 $\times$ 06		97.00
2,000	320 $\times$ 64 $\times$ 07	80.40	31.10
2,000	320 $\times$ 64 $\times$ 08	80.00	26.00

R_e	DG/CG	$K_x \times K_y \times N$	Time
10,000	DG	$040 \times 08 \times 06$	Crashed
10,000	DG	$080 \times 16 \times 06$	4.00
10,000	DG	$160 \times 32 \times 06$	80.00
10,000	DGc	$040 \times 08 \times 06$	Crashed
10,000	DGr	$040 \times 08 \times 09$	10.14
10,000	DGr	$082 \times 18 \times 06$	80.00
10,000	DGr	$082 \times 18 \times 07$	80.00
10,000	DGr	$082 \times 18 \times 08$	21.36
10,000	DGr	$082 \times 18 \times 09$	33.86
10,000	DGr	$162 \times 34 \times 06$	80.00
10,000	DGr	$400 \times 81 \times 09$	80.00
10,000	CG	$320 \times 64 \times 06$	97.00
10,000	CGr	$400 \times 81 \times 08$	80.00

Table: table of experiments for $R_e = 10,000$

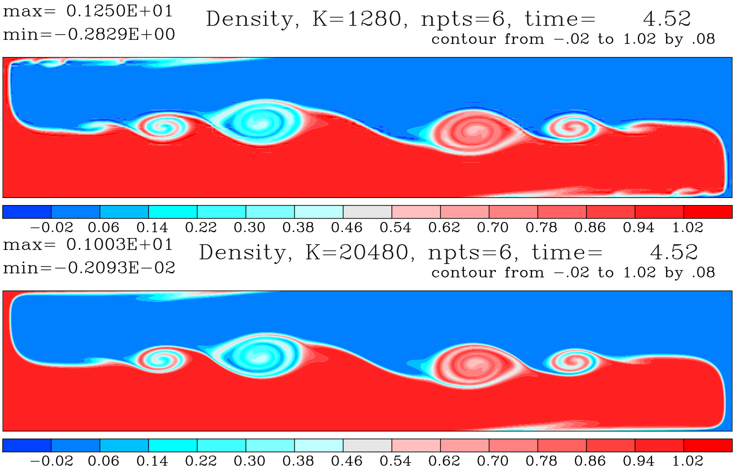

Figure: *h*-refinement DG density fields for Re=2,000

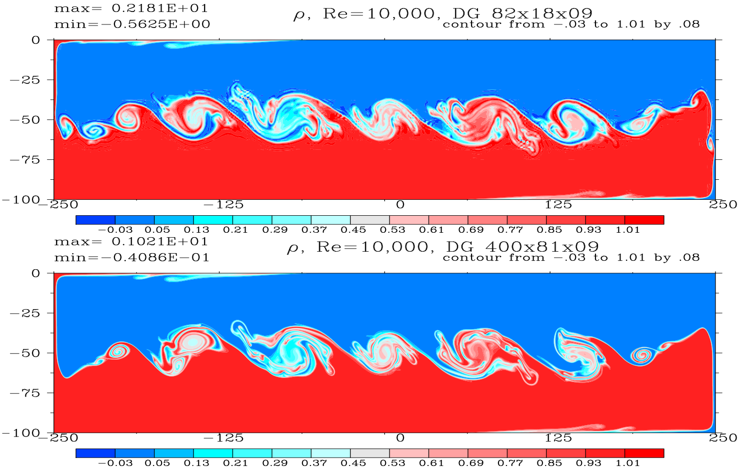

Figure: *h*-refinement DG density fields for Re=10,000

Out of range metric, $R_e = 2,000$

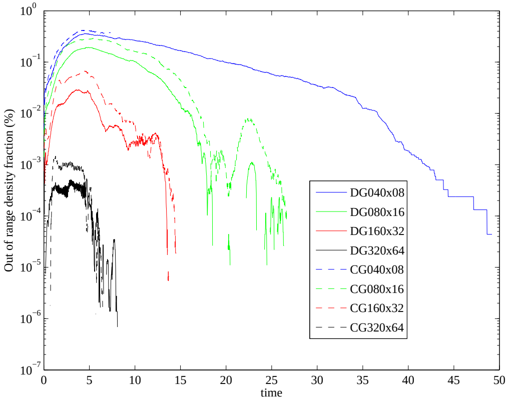

Figure: Out of range density fraction PDF for various CG and DG partitions at $N = 5$. The CG has a larger out of range fraction then DG for all cases except for the initial phase of the high resolution simulation with 320×64 partition.

Out of range metric, $R_e = 10,000$

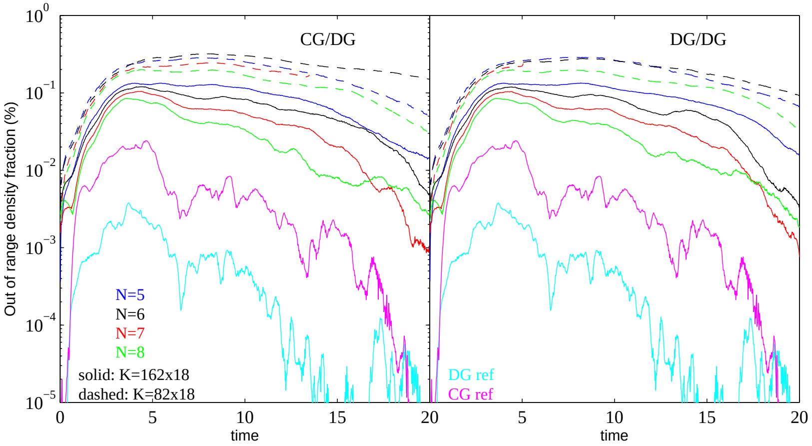

Density Classes comparison at t=80, $Re = 2,000$

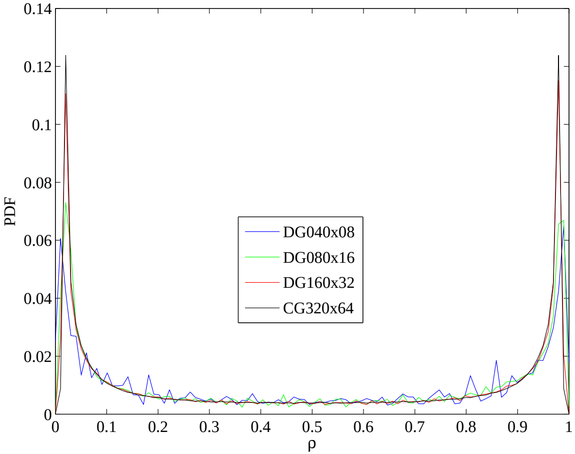

Figure: density PDF for the various runs for $N = 5$.

Errors in water mass pdf at t=20, $R_e = 10,000$

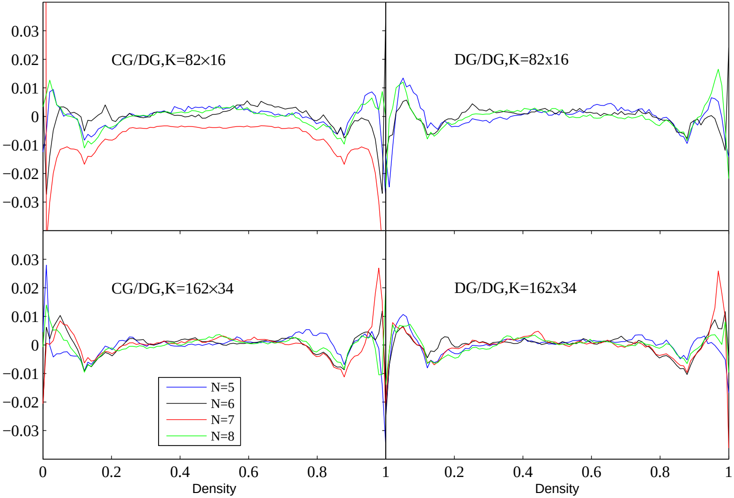

Figure: Errors in pdf relative to CG reference

Energy history of reference simulation $R_e = 2,000$

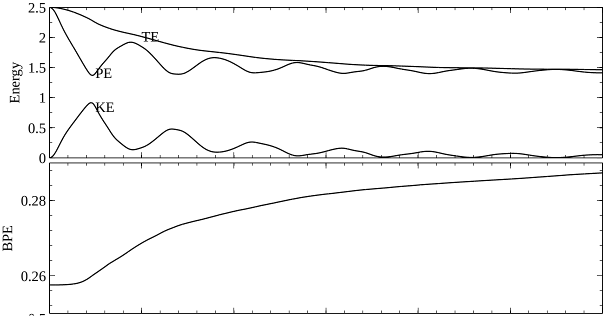

Figure: Energy history for reference CG discretization at $N = 5$.

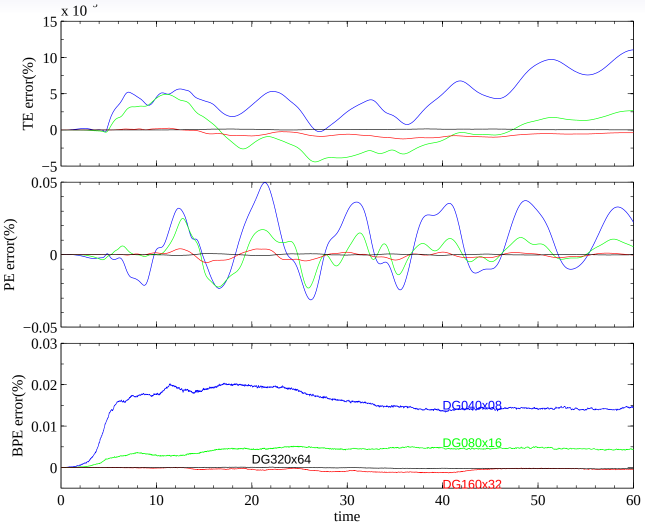

Figure: Energy error histories for various DG discretization at $N = 5$.

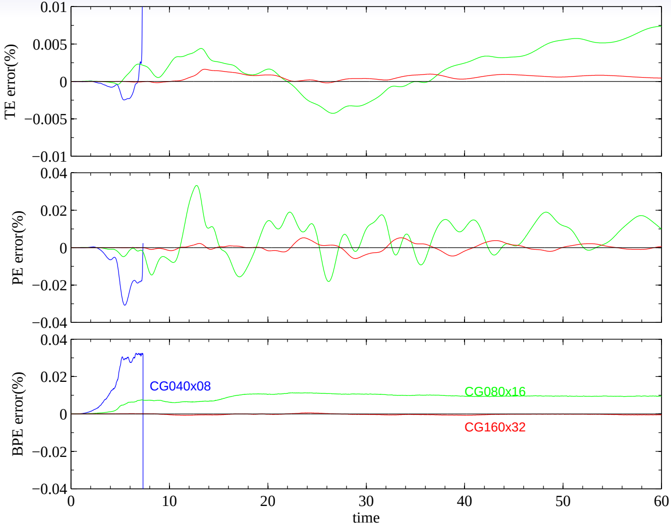

Figure: Energy error histories for various CG discretization at $N = 5$.

Energy errors for $R_e = 10,000$

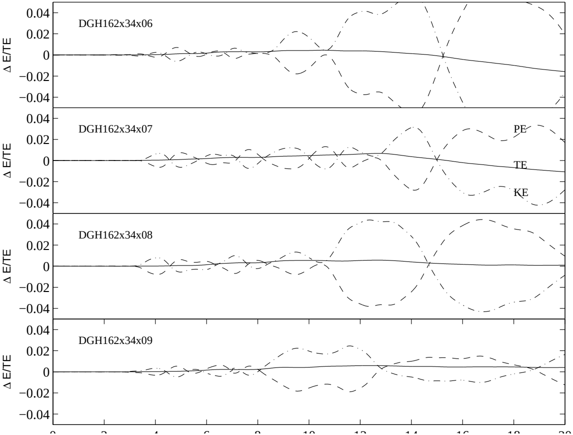

Figure: Energy errors normalized by TE of reference solution for a density DGM solution using 162×34 elements.

Conclusion for mixing

- Developed a model for gravity current mixing
- DGM discretization helps stabilize the model without excessive dissipation
- water mass properties impacted more then energy

Iterative Solvers

1. currently substructuring (Schur complement)
2. Call standard libraries PETc
3. Tailored solver for current geometry

Domain Decomposition into K rectangles

$$\Omega_k = [x_{k-1}\; x_k] \times [-1\; 0],\; k = 1, 2, \ldots, K$$

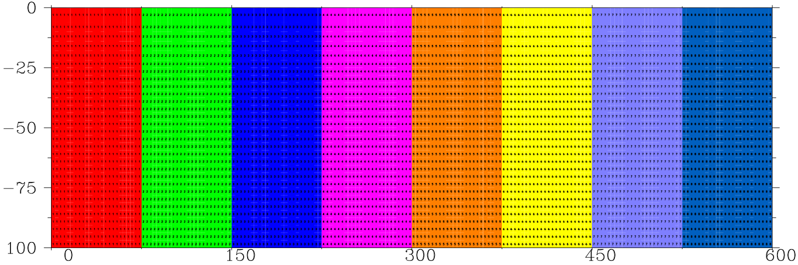

Local Poisson problems

$$\nabla^2 \psi^k = -\omega^k \text{ in } \Omega_k \tag{4}$$
$$\psi^k(x,0) = \psi^k(x,-1) = 0 \tag{5}$$
$$\psi^1(x_0,z) = \psi^K(x_K,z) = 0 \tag{6}$$
$$\psi^k(x_k,0) = \psi^{k+1}(x_k,z),\ k = 1,2,\ldots,K-1 \tag{7}$$
$$\psi_x^k(x_k,0) = \psi_x^{k+1}(x_k,z),\ k = 1,2,\ldots,K-1 \tag{8}$$

Equations 7 and 8 express the transmission conditions, namely the continuity of the function and its first derivative, across the $K-1$ internal boundaries located at x_k.

Domain Decomposition:Split Solution $\psi^k = \hat{\psi}^k + \overline{\psi}^k$

1. Poisson problem

$$\nabla^2 \hat{\psi}^k = -\omega^k \text{ in } \Omega_k \tag{9}$$
$$\hat{\psi}^k(x,0) = \hat{\psi}^k(x,-1) = 0 \tag{10}$$
$$\hat{\psi}^k(x_{k-1},z) = \hat{\psi}^k(x_k,z) = 0 \tag{11}$$

2. Laplace problem

$$\nabla^2 \overline{\psi}^k = 0 \text{ in } \Omega_k \tag{12}$$
$$\overline{\psi}^k(x,0) = \hat{\psi}^k(x,-1) = 0 \tag{13}$$
$$\overline{\psi}^k(x_{k-1},z) = \alpha^{k-1}(z) \tag{14}$$
$$\overline{\psi}^k(x_k,z) = \alpha^k(z) \tag{15}$$

Analytical solution to Laplace problem

$$\overline{\psi}^k(x,z) = \sum_{n=1}^{\infty} \frac{\alpha_n^{k-1}\sinh\lambda_n(x_k - x) + \alpha_n^k \sinh\lambda_n(x - x_{k-1})}{\sinh\lambda_n l_k} \sin\lambda_n z$$

$$\alpha_n^k = \frac{\displaystyle\int_{-1}^{0} \alpha^k(z)\sin\lambda_n z \, dz}{\displaystyle\int_{-1}^{0} \sin^2\lambda_n z \, dz}$$

$$\lambda_n = n\pi, \; n = 1, 2, \ldots$$

$$l_k = x_k - x_{k-1}.$$

Constraints on α^k

$$\left.\frac{\partial \overline{\psi}^{k+1}}{\partial x}\right|_{x_k} - \left.\frac{\partial \overline{\psi}^{k}}{\partial x}\right|_{x_k} = -\left(\left.\frac{\partial \hat{\psi}^{k+1}}{\partial x}\right|_{x_k} - \left.\frac{\partial \hat{\psi}^{k}}{\partial x}\right|_{x_k} \right) \tag{16}$$

$$\frac{\alpha_n^{k-1}}{\sinh \lambda_n l_k} - \left[\frac{\cosh \lambda_n l_k}{\sinh \lambda_n l_k} + \frac{\cosh \lambda_n l_{k+1}}{\sinh \lambda_n l_{k+1}}\right] \alpha_n^k + \frac{\alpha_n^{k+1}}{\sinh \lambda_n l_{k+1}} = -\frac{\beta_n^k}{\lambda_n}$$

$$\beta_n^k = \frac{\int_{-1}^{0} \left[\hat{\psi}_x^{k+1}(x_k, z) - \hat{\psi}_x^{k}(x_k, z)\right] \sin \lambda_n z \, dz}{\int_{-1}^{0} \sin^2 \lambda_n z \, dz}.$$

External interfaces require that $\alpha_n^0 = \alpha_n^K = 0$.
Symmetric tridiagonal system for each vertical mode n;
Redundant parallel solution.
Cut-off n? depends on β_n^k.
For large $\lambda_n l_k >> 1$ the off-diagonal terms asymptote to zero
Diagonal term asymptotes to 2

Domain Decomposition Algorithm

1. Solve inhomogeneous Poisson problem for $\hat{\psi}^k$.
2. Compute normal flux jump at internal interfaces $\left[\hat{\psi}^k_x\right]$
3. Compute Fourier-sine coefficients: $\beta^k_n = S\left[\hat{\psi}^k_x\right]$
4. Broadcast β^k_n to all processors
5. Solve tridiagonal systems on all processors $\alpha^k_n = T^{-1}\beta^k_n$.
6. Compute interfacial solution $\alpha^k = S^T\alpha^k_n$
7. Solve local Laplace problems

Domain Decomposition Algorithm

1. Schur complement problem: $\alpha^k = S^T T^{-1} S \left[\hat{\psi}_x^k\right]$
2. When geometry is not rectangular the above provide for symmetric preconditioner for the Schur complement problem.

Weak scalability analysis

K_x	K_y	NPROC	time
64	8	4	0.0758
96	8	6	0.1197
160	8	10	0.1572
176	8	11	0.1707
192	8	12	0.2339
240	8	15	0.2116
288	8	18	0.1583

Table: Scalability for 128 elements/processor

Analytical solution of tridiagonal system for $l_k = l$

Define Fourier-sine transform along the partition index:

$$\begin{pmatrix} \alpha_n^k \\ \beta_n^k \end{pmatrix} = \frac{2}{K} \sum_{m=1}^{K-1} \begin{pmatrix} \hat{\alpha}_n^m \\ \hat{\beta}_n^m \end{pmatrix} \sin \frac{\pi k m}{K} \tag{17}$$

Orthogonality of the functions $\sin \frac{\pi k m}{K}$:

$$\hat{\alpha}_n^m = \frac{\hat{\beta}_n^m}{2\lambda_n \left[\coth \lambda_n l - \sinh^{-1} \lambda_n l \cos \frac{m\pi}{K}\right]}. \tag{18}$$

Analytical solution of tridiagonal system for $l_k = l$

$$\begin{aligned}
\alpha_n^k &= \frac{2}{K}\sum_{m=1}^{K-1}\frac{\hat{\beta}_n^m}{2\lambda_n\left[\coth\lambda_n l - \sinh^{-1}\lambda_n l\cos\frac{m\pi}{K}\right]}\sin\frac{\pi km}{K} \\
&= \sum_{j=1}^{K-1}\underbrace{\frac{1}{\lambda_n K}\sum_{m=1}^{K-1}\frac{\sin\frac{\pi km}{K}\sin\frac{\pi jm}{K}}{\left[\coth\lambda_n l - \sinh^{-1}\lambda_n l\cos\frac{m\pi}{K}\right]}}_{B_{jk}^n}\beta_n^j
\end{aligned}$$

where the matrix B_{jk}^n is the inverse of the tridiagonal matrix.

Analytical solution of tridiagonal system for $l_k = l$

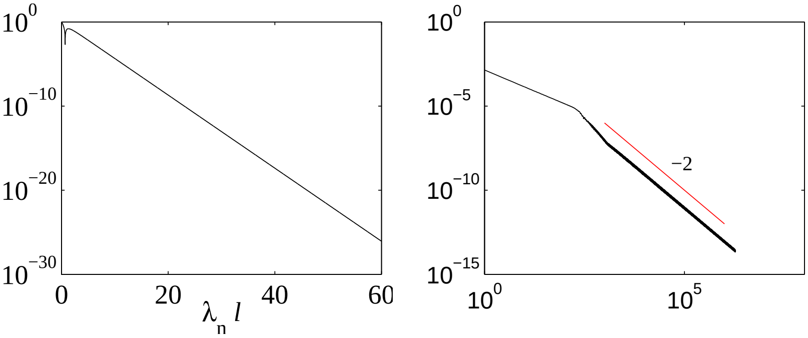

Left: $|\frac{\sinh \lambda_n l}{\cosh \lambda_n l - 1} - 1|$ versus n

Right: $\frac{1}{2\lambda_n}|\max_{1 \le i \le N}(|C^{e,k}_{i,n}|, |S^{e,k}_{i,n}|)$ versus n.

Computation of Fourier-sine coefficients

$$
\begin{aligned}
\beta_n^k &= 2\int_{-1}^{0}\left[\hat{\psi}_x^k(x_k, z)\right]\sin\lambda_n z \, \mathrm{d}z \\
&= \sum_{e=1}^{E}\Delta z_e\int_{-1}^{1}\left[\hat{\psi}_x^k(x_k, \sigma)\right]\sin\lambda_n\left(\Delta z_e\frac{\sigma+1}{2}+z_{e-1}\right)\, \mathrm{d}\sigma\beta_n^k \\
&= \sum_{e=1}^{E}\sum_{i=1}^{N}\left(C_{i,n}^{e,k}\cos\lambda_n\bar{z}_e + S_{i,n}^{e,k}\sin\lambda_n\bar{z}_e\right)\left[\hat{\psi}_x^k(x_k, z_i^e)\right] \\
C_{i,n}^{e,k} &= \Delta z_e\int_{-1}^{1}h_i(\sigma)\sin\frac{\lambda_n\Delta z_e\sigma}{2}\, \mathrm{d}\sigma \\
S_{i,n}^{e,k} &= \Delta z_e\int_{-1}^{1}h_i(\sigma)\cos\frac{\lambda_n\Delta z_e\sigma}{2}\, \mathrm{d}\sigma
\end{aligned}
$$

Computation of Fourier-sine coefficients

$$h_i(\sigma) = \sum_{m=0}^{N-1} h_{i,m} P_m(\sigma) \tag{19}$$

$$C_{i,n}^{e,k} = \Delta z_e \sum_{m=0}^{N-1} h_{im} \int_{-1}^{1} P_m(\sigma) \sin \frac{\lambda_n \Delta z_e \sigma}{2} \, d\sigma \tag{20}$$

$$S_{i,n}^{e,k} = \Delta z_e \sum_{m=0}^{N-1} h_{im} \int_{-1}^{1} P_m(\sigma) \cos \frac{\lambda_n \Delta z_e \sigma}{2} \, d\sigma \tag{21}$$

P_m: Legendre polynomial of degree m.
h_{im}: m-th Legendre spectral coefficient of $h_i(\sigma)$

Computation of Fourier-sine coefficients

$$C_{i,n}^{e,k} = 2\Delta z_e \sum_{m=1,3,5}^{N-1} (-1)^{\frac{m-1}{2}} \, h_{im} \, j_m\left(\frac{\lambda_n \Delta z_e}{2}\right) \tag{22}$$

$$S_{i,n}^{e,k} = 2\Delta z_e \sum_{m=0,2,4}^{N-1} (-1)^{\frac{m}{2}} \, h_{im} \, j_m\left(\frac{\lambda_n \Delta z_e}{2}\right) \tag{23}$$

Inverse Projection:Fourier-sine to Spectral element space

$$u(z) = \sum_n \hat{u}_n \sin \lambda_n z = \sum_{i=1}^{N} u_i h_i(z) \quad z_{e-1} \leq z \leq z_e$$

The matrix equations for the Fourier coefficients become

$$Mu = b \tag{24}$$

$$b_j = \sum_n \hat{u}_n \int_{z_0}^{z_E} h_j(z) \sin \lambda_n z \, \mathrm{d}z \tag{25}$$

$$= \sum_n \hat{u}_n \sum_e \frac{1}{2} \left[C^e_{j,n} \cos \lambda_n \bar{z}_e + S^e_{j,n} \sin \lambda_n \bar{z}_e \right] \tag{26}$$

M is 1D mass

$C^e_{j,n}$ and $S^e_{j,n}$ are as before

Solver Development Conclusion

- Validated transformation between SE and sine-spaces
- Developed and tested solver
- initial scalability tests promising
- room for improvement
- Compare specialized solver performance to other methods